Tuning composition of plasma activated water generated by transient spark discharge with electrospray

Pankaj Pareek[1], Saeed Kooshki[1], Peter Tóth[1], and Mário Janda*[1]

[1]Faculty of Mathematics, Physics, and Informatics, Comenius University in Bratislava, Mlynská dolina F2, 842 48 Bratislava, Slovakia

Abstract

Plasma-activated water (PAW) with a mixture of reactive oxygen and nitrogen species (RONS) has a wide range of applications in the health, agriculture, and the food sectors. However, some applications require PAW with a specific chemical composition. Therefore, we studied the generation of PAW by transient spark (TS) discharge in different gases (N_2, O_2, and synthetic air, dry or humidified) with direct or indirect contact of the discharge with water microdroplets formed by electrospray (ES) process. In direct contact, ES microdroplets were generated within the discharge zone. In the indirect treatment, the gas was first treated by TS discharge and sprayed by ES water microdroplets in the second section of the reactor. Using direct or indirect treatment, different inlet gas and input energy density, PAW with different composition was generated. Moreover, the obtained results allowed us to better understand the processes of PAW formation. H_2O_2(aq) is mainly formed due to short-lived reactive species, such as the OH radicals, and not by dissolution of gaseous H_2O_2. Next, NO_2^-(aq) ions are formed predominantly by the dissolution of gaseous HNO_2.

Keywords: plasma activated water, transient spark discharge, low temperature plasma, electrohydrodynamic spray, nitrites, hydrogen peroxide

*Corresponding author. Tel: +421-2-60295-520. E-mail: janda1@uniba.sk (Mário Janda)

1. Introduction

Non-thermal plasma is a flexible tool for addressing issues related to human and environmental well-being. Cold/non-thermal plasma produces high-energy electrons that induce significant chemical activity, making non-thermal plasma suitable for biomedical applications, water treatment, and even air cleaning [1-5]. The reactive chemical species in the plasma can be trapped in liquids/water to produce a chemically rich solution called plasma-activated water (PAW) or plasma-treated liquid [6]. PAW has been extensively studied to have a wide range of applications in food, agriculture, and biomedicine [2], [4], [6-8].

The high chemical reactivity of PAW can be attributed to the presence of various short- and long-lived reactive oxygen and nitrogen species (RONS) [6-9]. The short-lived species produced in PAW include nitric oxide (NO), superoxide (O_2^-), ozone (O_3), hydroxyl radical (OH), peroxynitrate ($OONO_2^-$) and peroxynitrite ($ONOO^-$) with lifetimes of less than one second. The long-lived species such as nitrates (NO_3^-), nitrites (NO_2^-) and hydrogen peroxide (H_2O_2) are much more stable in PAW.

In a typical air plasma in contact with water, a mixture of these species is commonly produced. However, for certain applications, only a few of these species are desirable, while others may play no role or even have negative effects [10]. For example, the reactive oxidizing species (ROS) such as H_2O_2, O_3, or OH radical play important roles in bacterial inactivation, targeting cancer cells, and improving the shelf life of foods such as fruits and vegetables [11-14]. On the contrary, reactive nitrogen species (RNS) such as NO_3^- and NO_2^- are beneficial for agricultural applications [15-17]. ROS are important products for advanced oxidation process for wastewater treatment [18], [19], instead RNS do not play a significant role in this process. Therefore, tuning the composition of PAW and selective production of desired RONS in plasma-activated water is very important for targeted and efficient applications of PAW [20].

Several authors have reported the selective production of RONS in PAW depending on the type of the discharge, reactor configuration, discharge polarity or power [21-23]. It was found that

low power (0.04-0.1 W/cm^2) surface dielectric barrier discharge (SDBD) resulted in O_3 as the dominant species, while high power (0.1-0.62 W/cm^2) SDBD resulted in the formation of nitrogen oxides [21]. Positive corona, negative corona, and dielectric barrier discharge in air were compared for the decontamination of metolachlor pesticide and negative corona was reported to have the highest efficiency due to higher OH and H_2O_2 concentration [22]. Machala et. al reported the dependence of the PAW composition on the discharge regime. Low power streamer corona discharge resulted mainly in the formation of H_2O_2 and O_3, while higher power transient spark discharge resulted in higher concentration of NO_3^- and NO_2^- [23].

When different gases are used, the gases dissolved in the liquid can also affect the RONS concentration in the produced PAW [24]. It was found that the presence of dissolved O_2 in water favors the formation of hydroxyl radicals compared to the water with air, while N_2 has a certain promoting effect on the formation of hydroxyl radicals, nitrites, and nitrates.

The chemical activity of PAW is also highly dependent on the type of interaction between the water and the plasma [25]. The transport rate of RONS from the gas to water microdroplets is faster than their transport rate to bulk water due to the increased surface area of the microdroplets [26], [27]. Numerous articles have been published on the interaction between plasma and microdroplets for bio-decontamination. For example, Ranieri et al. treated aerosolized microdroplets in a dielectric barrier discharge (DBD) reactor to decontaminate *E. coli* bacteria in a 100 L volume chamber [28]. Several researchers have chosen to treat the liquid in bulk and then aerosolize or electrospray the treated liquid to decontaminate small and uneven surfaces [29], [30].

The electrohydrodynamic spray of liquids, here simply called electrospray (ES), is a simple process to generate microdroplets from a bulk liquid by means of a strong electric field [31], [32]. In addition to bio-decontamination, ES has a high potential in many other areas, such as thin film deposition [33], wet electrostatic scrubbers for submicron particle removal [34], or inkjet printing systems [35].

The formation of ES microdroplets from water requires a relatively strong electric field, leading to the generation of electric discharges near the nozzle [36]. DC discharges such as corona, streamer corona, and transient spark discharge thus open the possibility of efficient production of highly reactive PAW by simultaneous generation of plasma and small microdroplets from the same high-voltage needle electrode [37-40].

Transient spark (TS) is a DC-driven self-pulsing discharge producing highly reactive non-thermal plasma for efficient generation of nitrogen oxides and nitrous acid [40-43]. In this work, TS and ES are used in two different reactor configurations. In the first configuration, TS and ES are generated together in the same section of the reactor. In the second configuration, the discharge section and the ES section are separated, i.e. the gas is first treated by TS discharge in the first section and then sprayed by ES water microdroplets in the second section of the reactor. In the first approach, both short-lived (OH, O_2^-, HO_2, ...) and long-lived (NO_2, HNO_2, H_2O_2, O_3) species generated in the plasma can play a role in formation of reactive species in water, while in the second approach only the long-lived species can reach the zone with the water microdroplets. In addition, the experiments were performed not only in dry and humidified synthetic air, but also in dry and humidified N_2 and O_2 gases separately, and at different discharge powers. The goal is to show how different experimental conditions can be used to tune the PAW composition by a single type of electrical discharge.

In this work, the concentrations of several gaseous and liquid products were measured. There are still relatively few works that sufficiently address the composition of both gaseous and liquid products in the formation of PAW [44]. The results obtained are therefore important for a better understanding of the formation mechanisms of reactive species in PAW and for assessing the role of different gas phase species in the formation of aqueous RONS. From a practical point of view, this knowledge will allow us in the future to increase energy efficiency and selectivity with respect to the desired products when generating PAW.

2. Materials and Methods

The experiments were conducted in a modular reactor containing either one or two sections for the generation of TS discharge and ES water microdroplets and a bottom section for water collection. Details of the reactor are discussed in the subsection 2.1. The generation of TS discharge and ES water microdroplets is explained in subsection 2.2. The analytical methods used are described in subsections 2.3 and 2.4.

2.1 Reactor details

Figure 1 shows a simplified schematic of the experimental system with the reactor. The reactor had a cylindrical geometry with an inner diameter of 35 mm, constructed using a Prusa MK3S+ 3D printer and using ABS (acrylonitrile butadiene styrene, a melting temperature between 220-245 °C, high mechanical strength) and PLA (polylactic acid, a melting temperature between 170-180 °C, very low deformability) as filament materials.

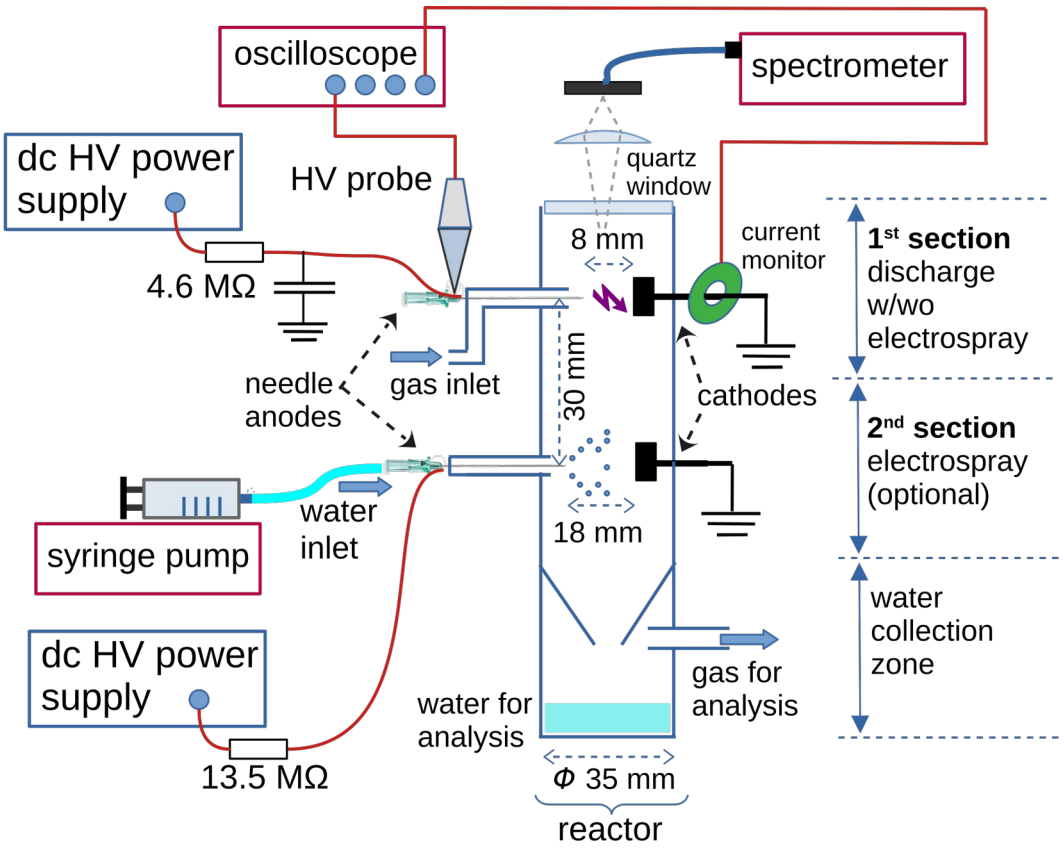

Figure 1 *- Simplified scheme of the experimental setup with the reactor having two sections (2SR), 1st section for TS generation, 2nd section for ES water microdroplets formation; HV - high voltage.*

The 3D printing technology allowed us to construct a modular reactor with sections that can be easily disassembled. The reactor can be used with two sections (2SR), with TS generation in the upper first section and ES microdroplets generation in the second section. Alternatively, TS discharge and ES microdroplets can be generated simultaneously in the first section and the second section can be removed. This configuration is referred to as a one-section reactor (1SR). In both sections, a steel M6 screw was used as the ground electrode (cathode) and a blunt stainless steel needle with an internal diameter of 0.6 mm was used as the high voltage electrode (anode). The needle was positioned opposite the M6 screw in a point-to-plane geometry. The distance between the electrodes in the first section was 8 mm, while the distance between the electrodes in the second section, which was used only to generate ES microdroplets, was 18 mm. The gas entered the reactor in the first section and flowed around the needle anode. The gas then passed through the second section, which was used to generate ES microdroplets. Both water and gas then entered the lower part of the reactor through a funnel-shaped junction. The water was then collected at the bottom of the reactor, while the gas exited the reactor through a small opening in the side wall of the reactor. Any leaks in the reactor were sealed with vacuum grease. Treated gases included dry and humidified O_2 (99.95% purity), dry and humidified synthetic air (80% N_2, 20% O_2, 99.99% purity), and humidified N_2 (99.99% purity) from cylinders (Linde Slovakia). A constant gas flow rate of 1 L/min was maintained for all experiments using a gas flow meter (Aalborg Instruments & Controls, Inc., model P single flow tube rotameter). Humidification was achieved by passing dry gases from the cylinders through a deionized water (conductivity less than 3 μS/cm) in a bubbler. Typically, a relative humidity of 94–96% was achieved, verified by a capacitive humidity sensor (Arduino).

2.2 Generation of discharge and water microdroplets

A high voltage (HV) DC power supply (Spellman SL30P300) connected to the needle electrode via series ballast resistor R = 4.6 MΩ was used to generate positive polarity TS discharge in the first section of the reactor. Despite the use of a DC power supply, TS is a self-pulsing discharge

due to the repetitive charging and discharging of the driving circuit capacitance C, with a typical repetition frequency f = 1–10 kHz [41], [42]. During the charging of the capacitance C, the voltage applied to the anode increases until it reaches a characteristic gas breakdown voltage V_{BR}. The gas breakdown, initiated by a streamer, allows a rapid discharging of the driving circuit capacitance and the formation of a short high current spark pulse.

The repetition frequency f of the transient spark process is given by the equation

$$f = \left[RC \times \ln\left(\frac{V_0}{V_0 - V_{BR}} \right) \right]^{-1}, \quad (1)$$

where V_0 is the input high voltage provided by the HV power supply.

The electrical characteristics of the TS discharge are measured with an HV probe (Cal Test Electronics CT4028) and a current monitor (Pearson Electronics 2877), and then processed with a digital oscilloscope (Tektronix TBS2104). The recorded waveforms are used to calculate an average breakdown voltage V_{BR}, and the repetition frequency f of the transient spark pulses.

According to equation (1), the frequency increases as the input high voltage increases. The TS discharge frequency can also be controlled by adjusting the average current supplied to the circuit by the HV power supply, while the applied voltage is above the breakdown voltage. Higher current means faster charging of the circuit capacitance and higher TS repetition frequency. The increase in f increases the input energy density E_d delivered by the transient spark discharge [45]. The input energy density is an important parameter to evaluate the energy efficiency of the formation of chemical products by TS discharge. The input energy density is the energy delivered per liter of input gas and can be calculated as

$$E_d = \frac{f \times E_p}{q} = P/q, \quad (2)$$

where q is the gas flow rate and P is the deposited power.

Energy delivered to the plasma per pulse E_p can be calculated from the measured breakdown voltage V_{BR}:

$$E_p = \frac{1}{2} C V_{BR}^2. \quad (3)$$

The total capacitance of the electrical circuit used to generate the TS in this work, $C = 66 \pm 6$ pF, was estimated by fitting the measured dependence of the TS repetition frequency on V_0 and V_{BR} according to formula (1). In the experiments presented in this paper, the TS repetition frequency was varied approximately in the range of 1-5 kHz by adjusting the average current supplied to the circuit by the HV power supply in the range of 0.7-2.5 mA. Consequently, the deposited power was varied in the range of 2-14 W, and the input energy density was varied in the range of 100-800 J/L, with an uncertainty of up to 25%. The main source of uncertainty was the determination of the repetition frequency and the average breakdown voltage. Therefore, several long scale voltage waveforms covering several hundred breakdown events were recorded for each experimental condition to minimize this uncertainty.

Precise repetition frequency could only be achieved by using different types of power supplies that generate short HV pulses at a predetermined frequency. However, the advantage of TS over discharges generated by short HV pulses is its ability to simultaneously generate plasma and water microdroplet electrospray. ES cannot be induced by short high voltage pulses applied to the needle. In TS, the electric field near the hollow needle tip is strong enough for microdroplets formation for most of the time between TS pulses [40].

To generate ES microdroplets directly in the discharge section (1SR), a deionized water (pH 5.8, conductivity <3 µS/cm) was continuously pumped into the reactor at a controlled flow rate of 500 µL/min through the HV needle anode in the first section of the reactor by a syringe pump (New Era NE-300). The needle was connected to the syringe pump by silicone tubing. To generate the electrospray in the second section of the reactor, the deionized water was pumped to the reactor by the syringe pump through the needle electrode in the second section of the reactor

(as shown in Figure 1), which was connected to a second high-voltage DC power supply (Spellman Bertan 210-30R) via a 13.5 MΩ resistor. The electrospray was operated at a constant voltage of 9 kV and the power needed to generate ES was approximately 0.2 W, for all experiments when ES water microdroplets were generated in the second section.

2.3 Spectroscopic tools for diagnostics of plasma and gases

The top opening of the first section of the reactor is enclosed by a quartz window. This enables to use optical emission spectroscopic technique for diagnostic of generated plasma. Time-integrated emission spectra of spark discharges were recorded by a two-channel compact emission spectrometer (Ocean Optics SD2000) with a 200-1100 nm range and resolution of 0.6-1.2 nm over this broad spectral region. The wavelength response of the spectrometer was calibrated by calibration lamp Avantes AvaLight-CAL-Mini.

To identify the emission lines in the spectra, the experimental spectra were compared with synthetic spectra of different atoms and ions (N, N^+, N^{++}, O, O^+, Fe, Fe^+, ...) calculated for different excitation temperatures, taking into account the line broadening by our spectrometer. Required spectroscopic constants were downloaded form NIST atomic spectra database [46]. For the calculation of synthetic spectra of molecular systems (NH A-X, N_2 SPS) we used Specair software [47]. Details are given in Supplement II.

The main analytical technique used to determine the composition of the gas after treatment was UV-Vis absorption spectroscopy, which is suitable for detection of NO, NO_2, O_3, and HNO_2. A deuterium lamp (Avantes AvaLight-D-S) was used as the light source and absorption spectra were measured with a spectrometer (Avantes AvaSpec-Mini4096CL) in the range 190-650 nm. The spectral resolution of this system is 0.5-0.7 nm. The absorption cuvette with length of 16 cm was used, with the absorption path 32 cm, achieved by using a mirror to make a double pass through the cuvette.

The concentration of RONS in the gas was obtained by fitting the measured absorption spectra with calculated 'synthetic' spectra. The synthetic UV-Vis spectra were calculated by our own

script using the Beer-Lambert law and absorption cross sections downloaded from the MPI-Mainz UV/VIS spectral atlas [48]. The downloaded absorption cross sections were convoluted to match the spectral resolution of our spectrometer. This approach was verified by measuring NO and NO_2 concentrations in calibration gas mixtures (1000 ppm of NO in N_2 and 1000 ppm of NO_2 in synthetic air, Linde Slovakia).

2.4 Liquid phase diagnostic tools

Colorimetric methods were used to quantify the amounts of NO_2^-(aq) and H_2O_2(aq) produced in water using the Shimadzu UV-1800 UV-Vis absorption spectrophotometer. Quantitative analysis of NO_2^-(aq) was performed using the Nitrate/Nitrite Colorimetric Assay Kit (#780001, Cayman Chemicals, Ann Arbor, MI, USA), which contains ready-to-use Griess reagents. Nitrites react with the Griess reagents, to produce a deep purple azo compound. The concentration of NO_2^-(aq) was calculated from the absorbance peak at 540 nm, using a calibration curve prepared by measuring the absorbance of standard NO_2^-(aq) solutions.

The concentration of H_2O_2(aq) was determined using the titanium oxy-sulfate $TiOSO_4$ assay under acidic conditions (4 g/L $TiOSO_4$ mixed in a 1:1 ratio with concentrated H_2SO_4) [49]. In this assay, titanyl ions Ti^{4+} react with H_2O_2(aq) to form a yellow colored compound known as pertitanic acid H_2TiO_4. The intensity of the color is directly proportional to the concentration of H_2O_2(aq). The concentration of H_2O_2(aq) was calculated from the absorbance peak at 407 nm, using a calibration curve prepared by measuring the absorbance of standard H_2O_2(aq) solutions.

After the discharge treatment, the sample was immediately stabilized with 60 mM sodium azide (NaN_3) to prevent removal of H_2O_2(aq) by its reaction with NO_2^-(aq) under acidic conditions. Sodium azide converts NO_2^-(aq) to molecular N_2 while maintaining the H_2O_2(aq) content [50]. The volume ratio of sample:NaN_3:$TiOSO_4$ was 10:1:5.

To estimate the concentration of OH(aq) radicals in treated water we used the fluorescence spectroscopic technique based on the reaction of terephthalic acid (TA) with OH(aq) radicals. This reaction results in the formation of hydroxyterephthalic acid (HTA). According to Mark et

al. [51], the yield of the TA reaction with the OH radical is 35 %. The TA solution (2 mM) was dissolved in a 5 mM NaOH solution (initial pH 10) because TA is only soluble in basic solvents. Since OH radicals have a lifetime in water below 4 µs [52], TA was added to the NaOH solution prior to treatment. A fluorescence spectrometer (Shimadzu RF-6000) was used to determine the concentration of HTA in solution after plasma treatment, with excitation and emission wavelengths of 310 nm and 425 nm, respectively [53]. The fluorescence intensity of the samples was compared with the fluorescence intensity of standard HTA solutions.

The concentration of NO_3^-(aq) was measured by two methods. First, an ion-selective probe (Horiba LAQUAtwin NO3-11) was used. Due to cross-sensitivity, the concentration of NO_2^-(aq) multiplied by a factor of 0.7, as recommended by the manufacturer, had to be subtracted from the obtained apparent concentration of NO_3^-. Second, the concentration of NO_3^-(aq) was also calculated by subtracting the concentration of NO_2^-(aq) from the concentration of NO_x^- (NO_3^- + NO_2^-), obtained by a colorimetric method using a reagent mixture of 10 mM 2,6-xylenol and acids (H_2SO_2:H_3PO_4 in a 1:1 ratio). The absorption maximum between 290 nm and 350 nm (Shimadzu UV-1800 UV-Vis absorption spectrophotometer) is directly proportional to the concentration of NO_x^-(aq) [54]. The concentration of NO_3^-(aq) was also estimated from the measured pH (portable pH/ORP meter WTW 3110), assuming equilibrium conditions between H^+, NO_3^- and NO_2^- ions. However, due to the low repeatability, large uncertainties and in many cases significantly different values shown by the three methods, NO_3^-(aq) concentrations are not reported in this paper. The amount of NO_3^-(aq) produced is only roughly compared to the amount of NO_2^-(aq).

3. Results and Discussion

The goal of the presented research is an efficient production of plasma activated water with desired composition. At the beginning of this endeavor is the ignition of the transient spark discharge and the study of its properties. Therefore, the presentation of the results starts with the

description of the TS discharge behavior in the studied gas mixtures with and without water electrospray (subsection 3.1). From a chemical point of view, the initial step in PAW production is the generation of short-lived, highly reactive radicals and ions in the plasma. The identification of these species by optical emission spectroscopy is described in subsection 3.2. Subsection 3.3 deals with the identification and quantification of long-lived gas-phase products. Finally, subsection 3.4 deals with the analysis of liquid phase products.

3.1 Electrical characteristics

The electrical characteristics of TS discharge in air at atmospheric pressure are well documented in our previous works [41], [42]. The electrical characteristics of TS generated simultaneously with ES of water microdroplets in air have also been reported [40]. Here we therefore focus on electrical characteristics of TS discharge generated in dry or humid O_2 and N_2, with and without water ES. These results are compared with the TS characteristics in synthetic air.

Figure 2a shows typical short-scale current and voltage waveforms of a transient spark discharge in humidified O_2 and humidified synthetic air, respectively, averaged over 128 shots, at power supply current of 1 mA. It is consistent with previously published results and confirms that TS in O_2 is also characterized by short high current pulses generated during the gas breakdown by rapid discharge of the total circuit capacitance [41], [42].

In fact, TS is based on repetitive charging and discharging of the driving circuit capacitance ($C = 66 \pm 6$ pF). Figure 2b shows a series of transient spark discharges occurring simultaneously with the generation of ES water microdroplets in O_2 (blue line) and in synthetic air (black line). We have demonstrated the ability of TS and ES to coexist in synthetic air in our recent work [40], where we found that TS and ES influence each other. This mutual influence causes instabilities of both ES and TS. For example, the water flow required for ES causes instabilities of TS, as shown in Figure 2b. There are periods of regular TS with breakdown voltage around 10 kV, but there are also periods when TS discharge is interrupted and the next breakdown and TS spark current pulse occurs only when the applied voltage exceeds 15 kV.

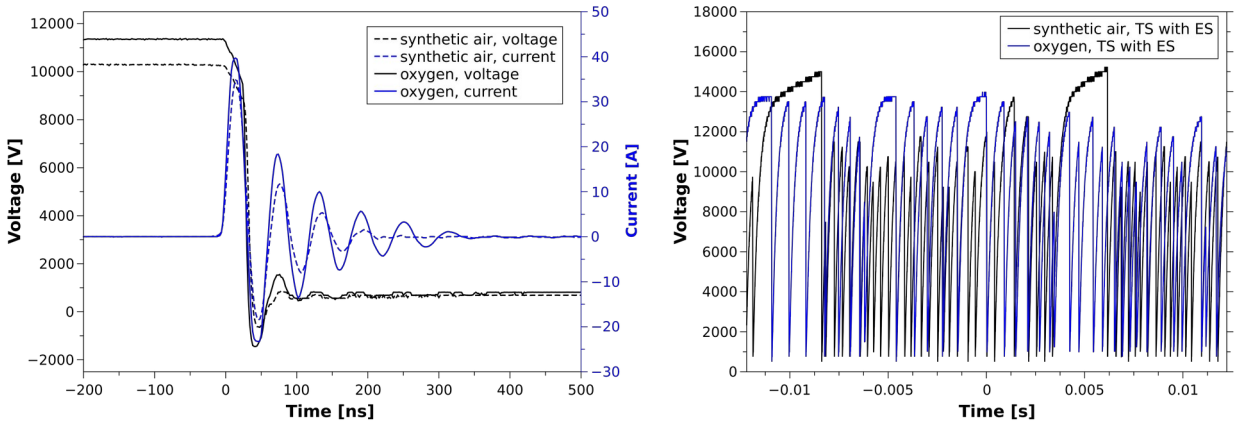

(a) (b)

Figure 2 *- Typical voltage and current waveforms of transient spark discharges in humidified O_2 and in humidified synthetic air; driving circuit capacitance of 66±6 pF, R = 4.6 MΩ, 8 mm gap; a) short time scale with focusing on spark current pulse and voltage drop during the gas breakdown; b) long time scale voltage waveforms of TS with ES, comparison of behavior in synthetic air and in O_2.*

Statistical analysis showed that at a power supply current of 1 mA, the TS discharge current pulses are repeated 80±5 % of the time with a relatively stable frequency of 2.4±0.8 kHz and a breakdown voltage of 10.5±1.1 kV. Periods without TS current pulses with an anode voltage above 12 kV represent about 20% of the time.

A different behavior was observed when TS discharges with ES microdroplets were generated in O_2 (Figure 2b, blue line). The breakdown voltage of TS with ES increased compared to the breakdown voltage without ES, from 11.9±0.4 kV to 13.6±0.6 kV (power supply current of 1 mA), but there are not such long periods without TS pulses and with anode voltage increasing up to 16 kV as in the synthetic air.

The discharge characteristics in humidified N_2 gas are similar to those in the synthetic air. However, in humidified nitrogen, the TS discharge is more prone to transition to a pulseless glow discharge than in air. The recharging of the driving circuit capacitance required to increase the anode voltage to reach the breakdown voltage again is only possible if the highly conductive plasma channel decays after the TS spark current pulse and the current flow through the gap stops. However, if the current supplied by the power supply is high enough, it can keep the

plasma channel active after the breakdown, thus preventing recharging of the driving circuit capacitance. In this case, TS switches to the glow discharge [55]. Under present conditions, the minimum current supplied by the HV power supply needed to sustain unstable glow discharge periods is about 1.5 mA in humidified N_2. In synthetic air, the TS discharge is still stable with a current of 2.5 mA supplied by the HV power supply.

In dry N_2 without ES, the stable TS discharge was not observed at all and the discharge rapidly switches to the pulseless glow discharge after a few TS spark current pulses. This behavior is probably due to the fact that in the absence of O_2 or H_2O molecules, there are no electron attachment reactions leading to the formation of negative ions (O^-, O_2^-, OH^-, H^-). The formation of negative ions in air plasmas reduces the concentration of free electrons and is an important factor in the decay of the plasma after the TS current pulse. In dry N_2, without the formation of negative ions, the electrons are not efficiently quenched and the plasma can be maintained even by glow discharge with a constant current of about 1 mA.

3.2 Optical characteristics

The emission spectra of the transient spark in air have already been presented in our previous works [42], [43]. As a novelty, we present here emission spectra of transient spark discharges operating in humidified N_2 and O_2 gases. Furthermore, we present here the influence of ES water microdroplets (500 µL/min) generated inside the discharge section on the optical emission spectra of the TS discharge. The current supplied by HV power supply was 1.1 mA.

Figures 3a and 3b show the normalized optical emission spectra of TS in humidified synthetic air, humidified N_2 and humidified O_2 gases in the spectral range of 200 to 515 nm and in the spectral range from 600 to 900 nm, respectively. The emission spectra of TS in humidified synthetic air in the 200-515 nm range are dominated by emission lines of N^+ and O^+ ions. It was also possible to identify emission bands of the second positive system (SPS) of the molecular nitrogen. It is likely that weak emission lines of N^{++} and O^{++} ions, as well as the NH (A-X) emission system, are also present in the spectra (Supplement II, Figures SII-1, SII-3 and SII-5).

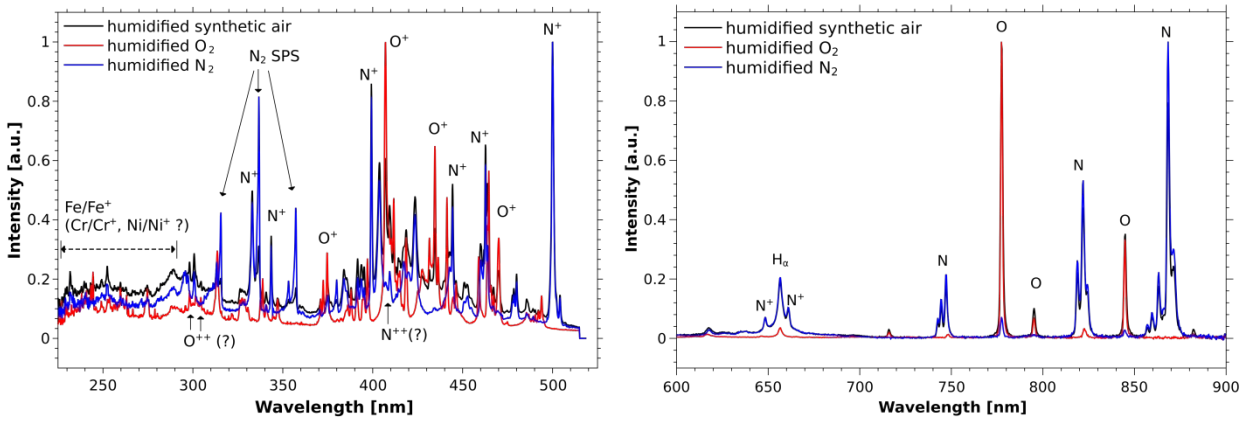

Figure 3 *- Normalized optical emission spectra of TS in humidified synthetic air, humidified O_2 and humidified N_2 gases in the spectral range from 200 to 515 nm (a); and in the spectral range from 600 to 900 nm (b).*

The fact that the spectra are dominated by N^+ and O^+ lines indicates a high degree of ionization during the high current pulse of the transient spark discharge. The emission spectra of TS in humid synthetic air in the 600-900 nm spectral region are dominated by emission lines of N and O atoms. The emission intensity of the H_α line near 656 nm is also relatively high. Several weak emission lines from N^+ ions are also present in this spectral region.

All of the above atomic and ionic emission lines and molecular emission bands are also present in the emission spectra of TS generated in humidified N_2. Of course, the emission lines of O and O^+ species are much weaker than in humidified synthetic air because molecular oxygen is not present in the inlet gas. O and O^+ species must be produced by dissociation of water molecules. For this reason, only the strongest lines of these species can be easily identified in the spectra shown, such as the O triplet line at 777 nm in Figure 5b. No emission lines of N and N^+ species, nor N_2 emission bands are found in the emission spectra of TS discharge in humidified O_2. Only the emission lines of O, O^+ and H species were identified.

In all gases, we also observed relatively weak emission lines of Fe and Fe^+ species in the spectral range of 200 to 280 nm. The presence of these emission lines can be attributed to the sputtering of the stainless steel needle anode. The intensity of Fe and Fe^+ emission lines changed

significantly in spectra obtained from experiments with simultaneous generation of TS discharge and ES water microdroplets.

Figure 4a shows a comparison of the optical emission spectra of TS in dry synthetic air with and without ES microdroplets and in humidified synthetic air in the spectral range from 215 to 515 nm. Spectra are normalized to the intensity of the N^+ ion emission line near 500 nm. Spectra of dry and humidified synthetic air without ES microdroplets are nearly identical, indicating no significant effect of humidity on TS discharge characteristics.

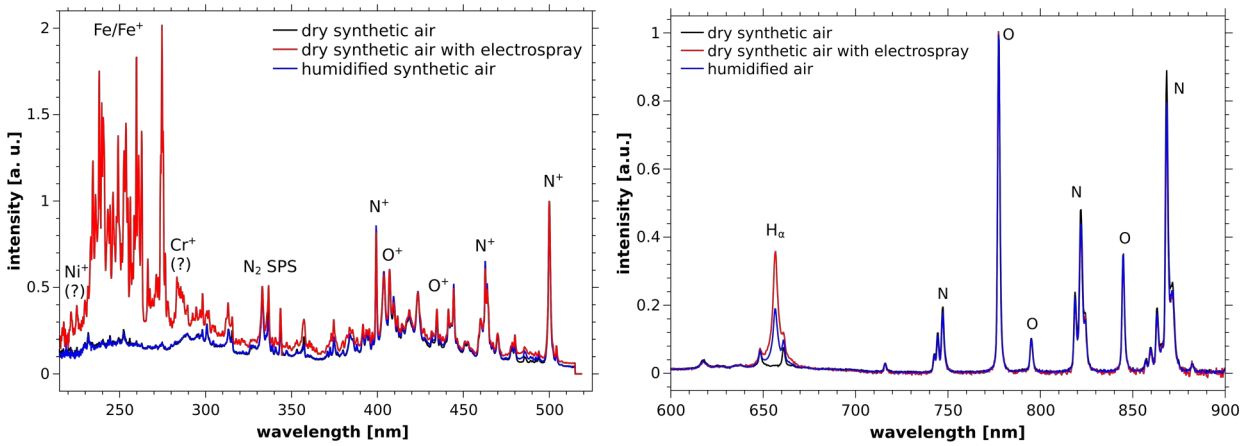

(a) (b)

Figure 4 *– Comparison of typical optical emission spectra of TS in dry synthetic air, dry synthetic air with ES microdroplets, and in humidified synthetic air; a) spectral range of 215-515 nm; b) spectral range of 600-900 nm.*

The emission spectrum of TS generated with ES water microdroplets is also very similar to the other two spectra, but only in the spectral region above 300 nm. Below 300 nm, the intensity of Fe and Fe^+ lines in the spectrum of TS with ES increased significantly compared to the spectra of TS without ES. There are probably also emission lines of Cr, Cr^+, Ni and Ni^+ species.

Figure 4b shows a comparison of the optical emission spectra of TS in dry synthetic air without and with ES microdroplets, and in humidified synthetic air in the spectral range from 600 to 900 nm. All spectra are normalized relative to the atomic oxygen triplet line near 777 nm, which was the strongest emission line in all three spectra. All three normalized spectra shown in

Figure 4b are nearly identical, the only exception being the intensity of the H_α line at 656 nm. The H_α line is absent in dry synthetic air. It is only present in air with water vapor or water microdroplets. Interestingly, the relative H_α line intensity is more than doubled in the spectrum of TS with ES microdroplets compared to the spectrum of TS in humidified synthetic air. The same differences between the spectra of TS with and without ES water microdroplets were observed when we used N_2 or O_2 gases.

The increase in H_α line intensity in the spectra of TS with ES microdroplets compared to the spectra of TS without ES in humidified gases is potentially interesting for plasma-activated water generation. The presence of the H_α line is mainly attributed to the impact of electrons on H_2O molecules [56]. Therefore, the increased H_α line intensity suggests that more H_2O molecules are dissociated into highly reactive H and OH radicals in TS with ES water microdroplets compared to TS in humidified gases. In a next step, OH radicals may dissolve in the water microdroplets where they can potentially form other reactive species such as H_2O_2.

The higher intensity of Fe and Fe^+ (and probably Cr/Cr^+, and Ni/Ni^+) lines indicates increased sputtering of the electrodes due to the presence of water flowing through the needle electrode. For this reason, we compared the damage to the needle anode after one hour of TS operation with and without the formation of ES water microdroplets.

(a) (b) (c)

Figure 5 *– The photos of the needle electrode tip; a) new electrode; b) electrode used for one hour to generate TS in dry air; c) electrode used for one hour to generate TS and ES microdroplets.*

Figure 5a shows a photograph of a new stainless steel needle with an almost flat and uniform tip. Figure 5b shows the tip of the stainless steel needle after one hour of TS discharge generation (1.3 mA supplied by the HV power supply). The current pulses in TS are short enough to avoid thermalization of the generated plasma, but the temperature is temporarily elevated above 2000 K during the short pulse phase [42]. This causes microscopic damage to the tip of the HV needle electrode. After one hour of operation, the burn marks with sharp edges are visible at the tip of the anode. Figure 5c shows a tip of the needle electrode after one hour of simultaneous generation of TS (1.3 mA supplied by the HV power supply) with ES water microdroplets at a water flow rate of 500 µl/min. A different type of erosion can be seen in Figure 5c. The electrode tip is smoothed by the action of the flowing water and there are no burn marks with sharp edges. The stronger intensity of the emission lines of metallic species in the emission spectra of TS with ES and smoothed edges indicates that the electrospray of water facilitates and enhances the sputtering of material from the tip of the anode.

The increased content of iron ions in the water can play an important role in the formation of the plasma activated water by TS in combination with ES water microdroplets. The presence of iron in the water can induce Fenton reactions causing the depletion of H_2O_2(aq). On the one hand, this could limit the maximum achievable concentration and lifetime of H_2O_2 in the generated PAW, but it is favorable for biomedical applications. The so-called Fenton reaction is a complex set of reactions between Fe and H_2O_2 generating both hydroxyl radicals and higher oxidation states of the iron, which are capable of oxidizing a wide range of substrates and causing biological damage [57].

3.3 Gas phase products

Optical emission spectra of TS in studied gas mixtures show production of various reactive atoms and ions in plasma. These atoms and ions initiate a rich set of reactions that can lead to the formation of various gaseous products (NO, NO_2, HNO_2, HNO_3, N_2O, N_2O_5, O_3, H_2O_2, ...). For

simplicity, let's start with description of gaseous products in experiments with dry O_2, where we can neglect species containing H and N atoms.

Ozone is the dominant long-lived gaseous product produced by TS discharge in dry O_2. It can be produced by reaction (4)

$$O + O_2 + O_2 \rightarrow O_3 + O_2 \qquad (4)$$

The formation of O_3 molecules most probably does not occur directly in the hot plasma filament generated by the spark current pulse due to the ozone thermal instability in hot discharge filaments [58]. The ozone is probably formed after the gas from the plasma channel containing O atoms is mixed with the surrounding colder gas containing O_2 molecules.

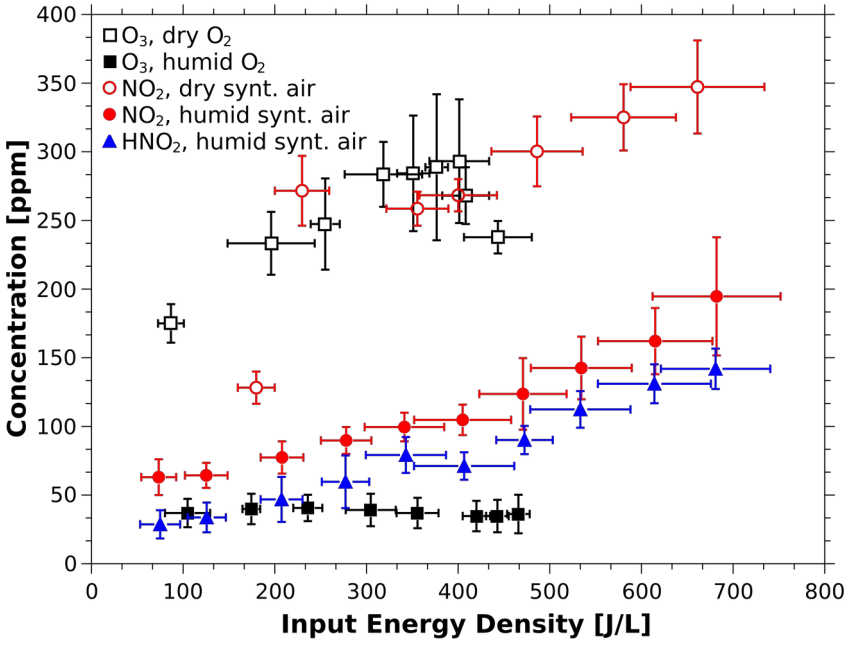

Figure 6 *– Concentrations of gaseous products in the outlet gas as functions of the input energy density E_d; O_3 generated in dry and humidified O_2, NO_2 and HNO_2 generated in dry and humidified synthetic air.*

Figure 6 shows the O_3 concentration in the treated gas as a function of the input energy density E_d. The O_3 concentration initially increases to about 300 ppm at $E_d \approx 400$ J/L. Further increase of the input energy density leads to decrease of the ozone concentration. This can be attributed to the increasing temperature of the treated gas with the increasing input energy density and the thermal instability of the O_3 molecules.

A different trend was observed when humidified O_2 was treated by TS discharge. A constant O_3 concentration of about 40 ppm was achieved, independent on the input energy density. This shows that water has dominant influence on O_3 production in the humidified O_2. First, OH radicals are formed by electron impact dissociation of H_2O molecules by reaction (5) and by reaction with $O(^1D)$ species (6) [59], [60]:

$$e + H_2O \rightarrow e + OH + H, \quad (5)$$

$$O(^1D) + H_2O \rightarrow OH + OH. \quad (6)$$

Next, OH radicals can initiate decomposition of O_3 by reactions (7) and (8) [61]:

$$OH + O_3 \rightarrow HO_2 + O_2, \quad (7)$$

$$HO_2 + O_3 \rightarrow OH + 2O_2. \quad (8)$$

The presence of OH radicals is important for the formation of H_2O_2 in the treated gases, for example by reaction (9) [62]:

$$OH + OH + M \rightarrow H_2O_2 + M. \quad (9)$$

Unfortunately, it is not possible to identify H_2O_2 in the UV-Vis absorption spectra. In order to estimate the concentration of H_2O_2 generated in the gas phase we therefore performed several measurements in which we placed a second bubbler with a de-ionized water at the outlet of the reactor. The solubility of H_2O_2 is so high that we can assume that practically all the H_2O_2 molecules produced by TS in humidified O_2 inside the reactor will dissolve in the water in the bubbler at the outlet. After 20 minutes of accumulation, we measured the concentration of H_2O_2(aq) in the water, and from the amount of dissolved H_2O_2 molecules we estimated the concentration of H_2O_2 in the gas leaving the reactor. We found that the concentration of H_2O_2 in the gas phase is only around 1-3 ppm.

In humid synthetic air, the concentration of O_3 at the outlet is negligible. The produced O_3 is consumed by reactions (7), (8), and by reaction (10) with NO:

$$NO + O_3 \rightarrow NO_2 + O_2. \quad (10)$$

Reaction (10) is so important that ozone is not detected at the outlet even in dry air, because the NO concentration in the synthetic air treated by TS discharge is very high. The concentration of NO increases with increasing input energy and it can exceed 1000 ppm at about 350 J/L [45]. The rate coefficient of the reaction (10) at 300 K is about 2×10^{-14} $cm^3.s^{-1}$ [63]. Assuming that O_3 is removed only by reaction (10) and there is a surplus of NO, at a constant concentration of 1000 ppm, the O_3 concentration should decrease exponentially with a characteristic decay time of about 2 ms. Thus, only a negligible amount of O_3 can reach cuvette where the treated gas is analyzed by UV-Vis absorption spectroscopic technique. Only when the input energy density is below ~100 J/L, the amount of NO produced is not sufficient to remove all O_3 molecules and some of them (<10 ppm) can remain in the air treated by TS discharge [45].

Despite being the dominant gas phase product, the solubility of nitric oxide is very low and NO does not play an important role in the generation of PAW by TS discharge [40]. Therefore, we focus here on the generation of the second and the third most abundant products, NO_2 and HNO_2, which are much more soluble in water than NO.

Figure 6 shows the dependence of the NO_2 concentration in the treated gas on the input energy density E_d in dry and humidified synthetic air. Higher amount of NO_2 was detected in dry synthetic air than in humid synthetic air. This could be explained by the NO_2 generation mechanism. Assuming that the majority of NO_2 molecules are produced by the reaction (10), the production of NO_2 depends on the amount of O_3 molecules produced in the treated gas. In humidified air, the O_3 molecules are depleted by reactions (7) and (8) and fewer O_3 molecules remain to oxidize NO to NO_2.

Lower concentration of NO_2 in humid air is compensated by formation of HNO_2, most likely by the following reaction

$$NO + OH + M \rightarrow HNO_2 + M. \quad (11)$$

The concentration of HNO_2 in humid air increases almost linearly with increasing input energy density and it is only by ~30% lower than the concentration of NO_2 in humid air (Figure 6). No HNO_2 was detected in dry synthetic air.

Although the main focus of this work is on the generation of plasma-activated water, it must be emphasized that valuable chemical products are also generated in the gas phase during the TS discharge. In humidified air, the TS discharge can be used as an alternative environmentally friendly source of HNO_2, with tunable concentration of HNO_2, without the need for additional valuable chemicals such as $NaNO_2$ or HCl.

3.4 Liquid products

For simplicity, let's start with the results of experiments using the carrier gases O_2 or N_2 (subsection 3.4.1). Without N_2, the formation of reactive nitrogen species can be neglected. Without O_2, reactive nitrogen species are expected to be the dominant products. When using synthetic air, we can generate PAW with a more complicated mixture of both reactive oxygen and nitrogen species, and these species may interact with each other, as discussed later in subsection 3.4.2.

3.4.1 Liquid products in experiments with the carrier gases O_2 and N_2

Figure 7 compares the concentration of H_2O_2(aq) in the collected water in 1SR and 2SR reactors, with the humidified O_2 and humidified N_2 as inlet gases. The concentration of H_2O_2(aq) in the water from the 2SR reactor with separate TS in the first section and ES in the second section is relatively low, below 100 µM in the case of humidified O_2. A similar concentration of H_2O_2(aq) was also detected when humidified N_2 is used, not shown in Figure 7. It is reasonable to assume that the low H_2O_2(aq) concentration in the water from the reactor with two separate sections is caused by relatively small amount of H_2O_2(g) formed by TS in the first section.

The concentration of H_2O_2(aq) in the PAW generated in the 1SR reactor with direct contact of TS discharge with ES microdroplets in the first section is significantly higher. In humidified O_2, the

concentration of H_2O_2(aq) gradually increases with increasing input energy density up to ~4000 µM. In humidified N_2 the concentration of H_2O_2(aq) is lower and reaches about 1500 µM. These results show that H_2O_2(aq) in the water in our system cannot be formed dominantly by solvation of H_2O_2(g) from the gas phase, as was shown in the literature [64]. We suggest that the formation of H_2O_2(aq) in the plasma-activated water is significantly influenced by short-lived species when water microdroplets interact directly with the TS discharge. For example, H_2O_2(aq) could be produced by direct solvation of OH radicals transported into the water, where they may undergo a 2-body reaction [65], [66]:

$$OH(aq) + OH(aq) \rightarrow H_2O_2(aq). \quad (12)$$

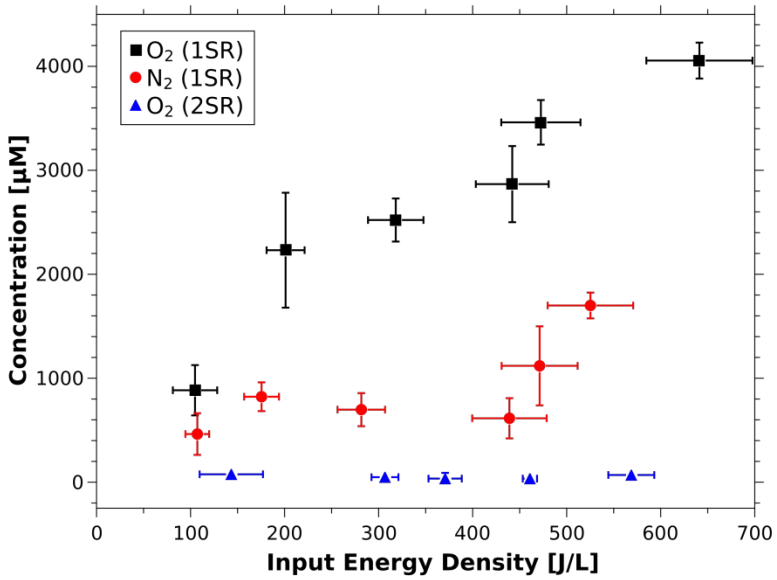

***Figure 7** - Concentration of H_2O_2(aq) as a function of input energy density; ES water flow rate 500 µl/min, duration of the experiment 2 minutes, 1SR reactor (TS and ES generated in the same section), 2SR reactor (TS in the 1st section, ES in the 2nd section of the reactor).*

The concentration of OH(aq) in the treated water was measured to verify the possible role of OH radicals in the formation of H_2O_2(aq). For this purpose, terephthalic acid (TA) was used as a fluorescent probe. TA is non-fluorescent, but readily undergoes hydroxylation upon contact with OH radicals, producing luminescent compounds known as hydroxy-terephthalic acid (HTA). Humidified or dry O_2 was used as the working gas to avoid the formation of reactive nitrogen species. In both systems, with reactor having either one or two sections, constant liquid flow rate

of 500 µL/min was used, and the mean input energy density was 130 ± 10 J/L. In addition, a control measurement was performed to test OH(aq) radical production solely by ES in the second section, without turning on the TS discharge in the first section of the reactor.

Figure 8 shows the concentration of OH(aq) radicals as derived from the concentration of HTA in the treated solutions. A small amount of OH(aq), was observed even in the solution from the control experiment without TS discharge, only with the formation of ES microdroplets in the second section (Figure 8, column d). This could be explained by the ignition of a weak corona discharge around the needle tip at an applied voltage of 9 kV, producing a small amount of OH radicals in the gas.

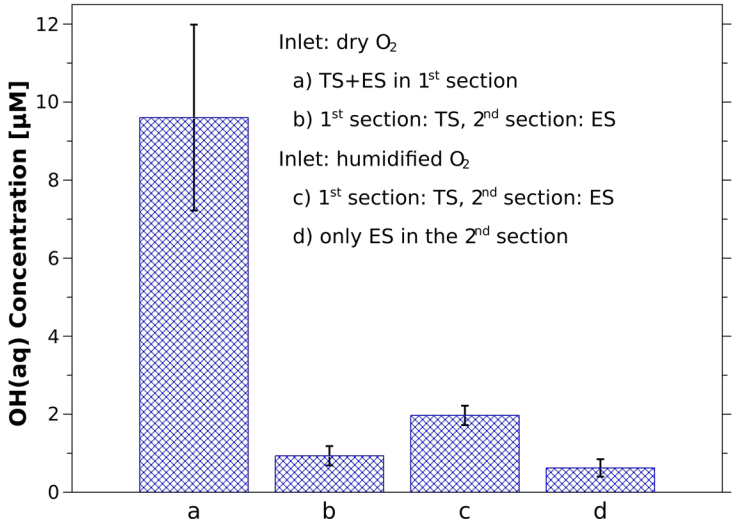

Figure 8 *– Concentration of OH(aq) radicals produced in 2 mM terephthalic acid (TA) solution, a) TS and ES together in the 1st section, b,c) TS in the 1st section, ES in the 2nd section, d) no TS discharge, only ES in the 2nd section; dry (a,b) or humidified (c,d)* O_2 .

The concentration of OH(aq) radicals in the solution from the 2SR reactor experiment in dry O_2 at the inlet is almost the same as in the control sample (Figure 8, column b). In dry O_2, the TS discharge in the first section of the reactor produces only weakly soluble O_3 in the gas phase and no other soluble species, e.g. H_2O_2, which could theoretically influence the formation of OH(aq) in the ES microdroplets in the second section of the reactor. Thus, the observed OH(aq) in 2SR in dry O_2 could only be produced by a weak corona accompanying the formation of ES

microdroplets. Therefore, it is reasonable to assume that the concentration of OH(aq) radicals in the solution from the experiment in 2SR and in dry O_2 at the inlet should be the same as in the control sample.

The concentration of OH(aq) is slightly higher in the solution from the experiment in the 2SR reactor in humidified O_2 (Figure 8, column c). Here, the TS discharge in the first section can produce a small amount of H_2O_2(g) that could be transported to the second section of the reactor. Solvation of H_2O_2(g) generated by TS in the first section can explain the slightly increased OH(aq) concentration compared to the control sample (ES without TS).

More important is the finding that the concentration of OH(aq) radicals is more than 4 times higher in the solution from the experiment where TS and ES microdroplets interact directly with each other in the first section of the reactor (Figure 8, column a). This result supports the hypothesis that at least some of the H_2O_2(aq) molecules are formed from OH(aq) radicals.

The concentration of OH(aq) is much lower (~10 μM) than the corresponding concentration of H_2O_2(aq), ~800 μM, obtained in 1SR reactor at an input energy density of about 100 J/L (Figure 7). Note that it is not correct to compare the results obtained under different experimental conditions, because the pH of the TA solution is higher than the pH of the treated deionized water. However, the concentration of H_2O_2(aq) is so much higher than the concentration of OH(aq) that it is very likely that some other short-lived species play a significant role in the formation of H_2O_2(aq) in the system with direct contact of water microdroplets with plasma.

H_2O_2(aq) can also be formed by a liquid phase reaction from dissolved HO_2 radicals [67], [68]

$$HO_2(aq) + HO_2(aq) \rightarrow H_2O_2(aq) + O_2, \quad (13)$$

or by a sequence of e and H^+ associative reactions (14) and (15):

$$HO_2(aq) + e(aq) \rightarrow HO_2^-(aq), \quad (14)$$

$$HO_2^-(aq) + H^+(aq) \rightarrow H_2O_2(aq). \quad (15)$$

Interaction of dissolved singlet state atomic oxygen $O(^1D)$ with H_2O molecules was also reported to form H_2O_2(aq) [69], [70]:

$$O(^1D)(aq) + H_2O \rightarrow H_2O_2(aq). \quad (16)$$

In humidified N_2, the concentration of H_2O_2(aq) in PAW is much lower compared to the PAW generated using humidified O_2 (Figure 7). According to Yang et al., different gases dissolved in the water can affect the RONS concentration in the produced PAW, but the H_2O_2(aq) concentration in PAW from their experiments using either water with dissolved O_2 or N_2 was the same (within the experimental error) [24]. Therefore, it is reasonable to assume that the different concentration of H_2O_2 in PAW from experiments in humidified N_2 and in humidified O_2 is not caused by dissolved O_2 and N_2 itself. It is more reasonable to assume that the production of reactive oxygen species (OH, $O(^1D)$, HO_2) species is lower in humidified N_2 than in humidified O_2, because O_2 molecules cannot contribute to their formation and they can only be produced from water molecules.

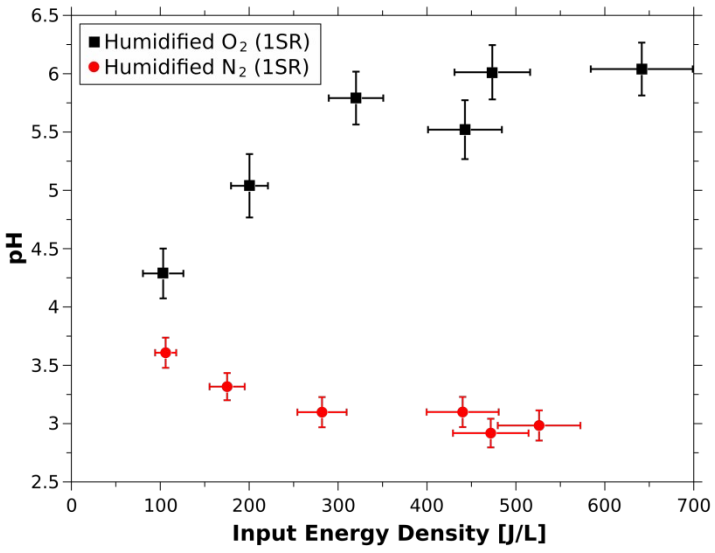

Figure 9 *– Influence of the input energy density on the pH evolution of PAW produced by TS and ES operated simultaneously in the first section of the rector (1SR) in humidified O_2 and N_2 gases.*

There is another possible explanation for the lower concentration of H_2O_2(aq) in PAW from the experiments in humidified N_2 compared to humidified O_2. In humidified N_2, NO_2^-(aq) was detected in most of the samples with a concentration within the ranging from 100 µM to 450 µM,

while in the humidified O_2, the concentration of NO_2^-(aq) was negligible. As a result, the pH of PAW generated in humidified N_2 decreases with increasing E_d (Figure 9).

Under acidic conditions, NO_2^-(aq) can decrease the concentration of H_2O_2(aq) through the following reactions [14], [48], [71]:

$$NO_2^-(aq) + H_2O_2(aq) \rightarrow NO_3^-(aq) + H_2O, \quad (17)$$

$$NO_2^-(aq) + H^+(aq) + H_2O_2(aq) \rightarrow ONOOH(aq) + H_2O, \text{ and} \quad (18)$$

$$NO_2^-(aq) + H^+(aq) + 2H_2O_2(aq) \rightarrow O_2NOOH(aq) + 2H_2O. \quad (19)$$

These reactions show that the humidified oxygen, without nitrogen, must be used for the most efficient production of H_2O_2(aq). On the other hand, these reactions show that for the production of ONOOH(aq) and O_2NOOH(aq), which play an important role for the antimicrobial effects of water [72], it is convenient to produce a mixture of H_2O_2(aq) and NO_2^-(aq) in the liquid phase, and in the gas phase we need N_2 in addition to O_2. From this point of view, the results obtained in synthetic air, which will be discussed in the next subsection, are interesting.

3.4.2 Generation of plasma-activated water in synthetic air

Figure 10a shows the dependence of the NO_2^-(aq) concentration on the input energy density in water from experiments in the 2SR reactor with the first section for generation of TS discharge and the second section for ES microdroplets formation. The working gas was either dry or humidified synthetic air.

In the 2SR system, only the long-lived products generated by the TS discharge in the first section can reach the second section where they can dissolve in the ES water microdroplets. In dry air, the main gas products are NO and NO_2. The formation of NO_2^-(aq) from the dissolved NO(aq) and NO_2(aq) proceeds by the following reactions

$$NO(aq) + NO_2(aq) + H_2O \rightarrow 2NO_2^-(aq) + 2H^+, \quad (20)$$

$$NO_2(aq) + NO_2(aq) + H_2O \rightarrow NO_2^-(aq) + NO_3^-(aq) + 2H^+. \quad (21)$$

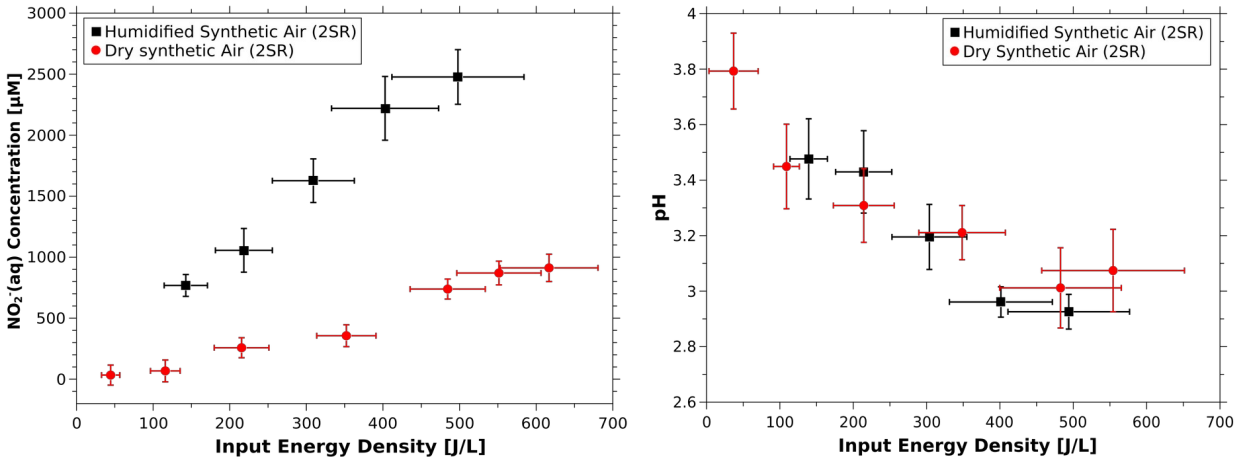

(a) (b)

Figure 10 *- Influence of the input energy density (a) on the concentration of NO_2^-(aq), and on the pH evolution (b) of the collected water; 2SR reactor (TS in the first section, ES in the second section).*

The NO_2 concentration generated by TS in the dry air is higher than the NO_2 concentration generated by TS in the humidified air (Figures 6). On the contrary, the concentration of NO_2^-(aq) in water from the humidified air experiments is much higher than in the water from dry air (Figure 10a). In humidified air, the contribution of HNO_2 must be taken into account:

$$HNO_2(g) \rightarrow HNO_2(aq) \leftrightarrow H^+ + NO_2^-(aq). \quad (22)$$

Obtained results thus prove important role of HNO_2 on NO_2^-(aq) formation in PAW generated by TS, because the solubility of HNO_2 in water is much higher than the solubility of NO_2.

The hypothesis that NO_2^-(aq) is formed in experiments in 2SR and humidified air dominantly by reaction (22) is also supported by the finding that the concentration of NO_3^-(aq) in the water is significantly lower than the concentration of NO_2^-(aq). When dry air is used, the concentration of NO_3^-(aq) is roughly the same as the concentration of NO_2^-(aq), indicating the dominant role of the reaction (21).

The production of H^+ by reactions (20) and (21) explains the acidification of the collected water (Figure 10b), i.e. the decrease in pH down to 2.9-3.1 with the increasing input energy density. At low pH, NO_3^-(aq) is also formed from NO_2^-(aq) by a disproportionation reaction [49]

$$3NO_2^-(aq) + 3H^+ \rightarrow 2NO(aq) + NO_3^-(aq) + H_3O^+. \quad (23)$$

However, if the initial pH is above 3.4, the decrease of NO_3^-(aq) concentration is relatively slow.

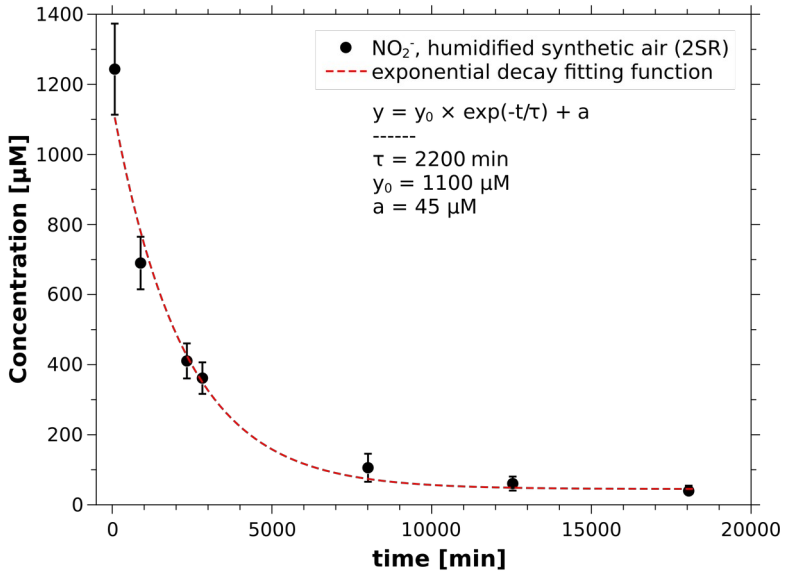

Figure 11 *– The evolution of NO_2^-(aq) concentration in the collected water from 2SR in humidified synthetic air, water flow rate 500 µl/min, experiment duration 2 minutes, initial pH ~3.4.*

Figure 11 shows the evolution of the NO_2^-(aq) concentration in the water produced in 2SR, with separated TS in the first section and ES in the second section, at an input energy density of about 220 J/l. The decrease of the NO_2^-(aq) concentration can be approximated by an exponential decay function with characteristic decay time of about 2200 minutes. The relatively long lifetime of NO_2^-(aq) can be attributed to a relatively high pH and a negligible concentration of H_2O_2(aq) in the collected water. Therefore, the disproportionation to NO_3^-(aq) by reaction (23) is relatively slow and the conversion of NO_2^-(aq) by reactions (17)-(19) can be neglected. The characteristic decay time of H_2O_2(aq) in PAW prepared in 1SR with O_2 gas with negligible concentration of NO_2^-(aq) is even longer, about 12000 minutes (more than 8 days).

The results are different when PAW is produced in the reactor where TS and ES are generated simultaneously in the first section of the reactor (1SR). The formation of H_2O_2(aq) is not negligible, because short-lived species such as OH, HO_2 and $O(^1D)$ radicals are likely to dissolve in water microdroplets as discussed in section 3.4.1.

Figure 12a shows the dependence of NO_2^-(aq) and H_2O_2(aq) concentrations on the input energy density in water from the 1SR experiments in humid synthetic air. The concentration of H_2O_2(aq)

decreases while the concentration of NO_2^-(aq) increases with the increasing input energy density. We assume that the H_2O_2(aq) concentration decreases with increasing input energy density due to increasing concentrations of NO and NO_2 in the gas. The nitrogen oxides react with OH radicals in the gas, thus less OH radicals can be dissolved in the microdroplets, and less H_2O_2(aq) is formed in the liquid phase by the reaction (12).

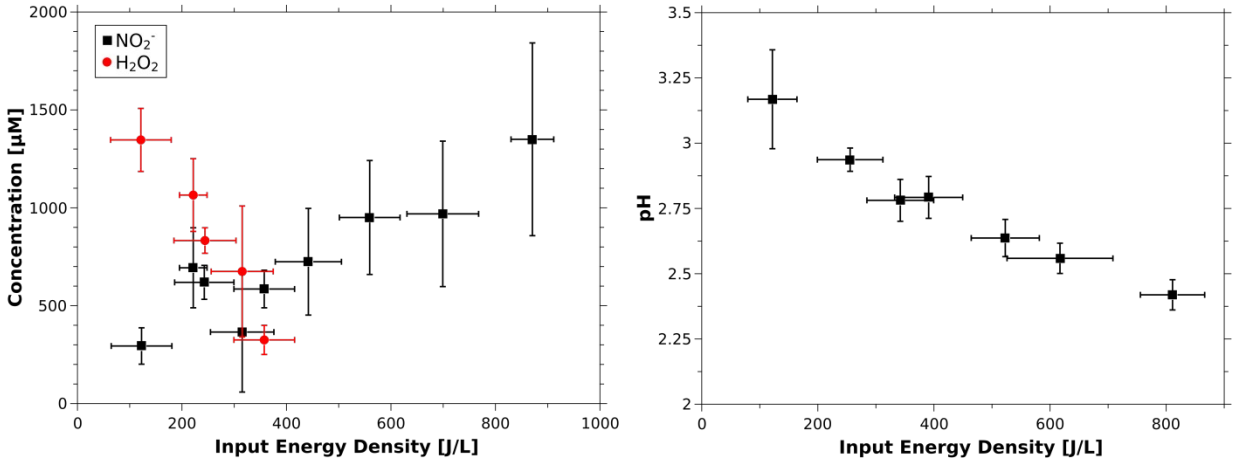

(a) (b)

Figure 12 *– Influence of the input energy density on the concentration of H_2O_2(aq) and NO_2^-(aq) (a) and on the pH evolution (b) of the collected water; 1SR (TS and ES generated simultaneously in the first section of the reactor).*

A mixture of NO_2^-(aq) and H_2O_2(aq) is present in PAW only when the input energy density is less than 400 J/L. PAW with a relatively high concentration of both NO_2^-(aq) and H_2O_2(aq) (600-800 µM) is generated at the input energy density of 200-300 J/L. PAW generated under these conditions can be used in applications exploiting its antibacterial properties thanks to the generation of ONOOH(aq) and O_2NOOH(aq) by reactions (18) and (19). Although it is still an open question how to define the dose of PAW and what is the dose-response relationship of PAW on cells, it was recently shown that H_2O_2 alone and the combination of H_2O_2 and NO_2^- played a significant role in cell death, while NO_2^- and NO_3^- alone had minimal effects [73].

Naturally, the mutual reactions gradually decrease the concentrations of both NO_2^-(aq) and H_2O_2(aq) in the generated PAW. At a pH below 3 (Figure 12b), NO_2^-(aq) can also be converted to NO_3^-(aq) by reaction (23). The presence of NO_3^-(aq) in PAW immediately after the

experiment was confirmed by the analytical techniques used. The concentration of NO_3^-(aq) is of the same order of magnitude as the concentration of NO_2^-(aq), most likely slightly higher.

Figure 13 shows the time evolution of NO_2^-(aq) and H_2O_2(aq) concentrations in PAW produced in 1SR, for an input energy density of ~250 J/L and the initial pH of ~2.9. The temperature of the PAW immediately after the treatment was ~30 °C, i.e. it increased by about 5 °C. The concentration of H_2O_2(aq) and NO_2^-(aq) decreases to about 50% of the initial value in 30-40 minutes. The time evolution of the concentrations of both species is very similar. This supports our hypothesis that NO_2^-(aq) and H_2O_2(aq) mostly react with each other through reactions (17)-(19). The concentration of NO_2^-(aq) decreases only slightly faster than the concentration of H_2O_2(aq), possibly due to a disproportionation reaction (23).

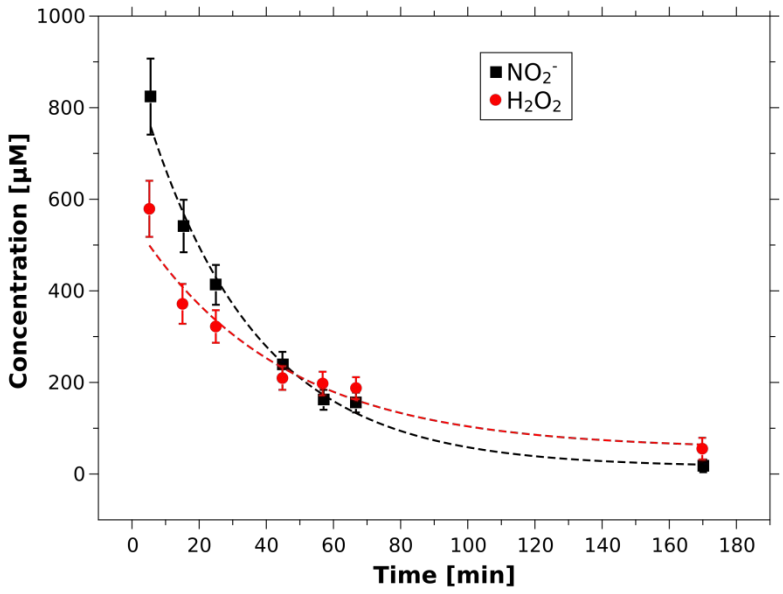

Figure 13 *– Time evolution of NO_2^-(aq) and H_2O_2(aq) concentrations in PAW with an initial pH of ~2.9, TS and ES generated simultaneously in the first section of the reactor in synthetic air; input energy density ~250 J/L.*

The biocidal effectiveness of PAW decreases in time due to decreasing concentrations of H_2O_2(aq) and NO_2^-(aq), although it was shown that PAW can retain bactericidal effects even after 18 months when stored at the -150 °C [74]. However, additional energy is required to freeze PAW for longer periods. Energy efficiency is one of the drawbacks of the PAW generation process that needs to be overcome [44], and freezing PAW would make it even worse.

In PAW without H_2O_2, the concentration of NO_2^-(aq) remains high for at least two days even at laboratory temperature and an initial pH of about 3.4 (Figure 11). With pH adjusted to above 4, it could probably be stored much longer in a refrigerator at 4 °C. The PAW containing mainly NO_2^- without H_2O_2 has no significant bactericidal effect and could not be used directly in biomedical applications. However, it could be stored longer and later mixed with a solution containing an appropriate concentration of H_2O_2 to achieve desired dose, e.g. defined as equivalent total oxidation potential [73].

In PAW from the 2SR system, with TS generation in the first section and ES in the second section of the reactor, we were also able to achieve a higher concentration of NO_2^-(aq) than in the 1SR system with, the simultaneous generation of TS and ES in the first section of the reactor. As a result, the energy efficiency of NO_2^- production was also better, about 2.5 nmol/J. This value is comparable or even better than in some other PAW generation systems [44],[75], [76], but better efficiency has also been reported [77]-[79]. For example, Xu et al. used for example low power corona discharge (0.05 W) and achieved the energy efficiency of NO_2^- production of about 66 nmol/J, but with a treatment time 60 min [77]. In our system is the interaction time of water microdroplets with plasma-treated humid air is very short and it can be used in continuous operation mode.

Note that the presented work is focused on basic research and better understanding of the processes behind the formation of plasma-activated water. The goal is to be able to tune the composition of the generated PAW on demand. The achieved energy efficiency can be significantly improved compared to the presented results in future research focused on energy efficiency optimization. In addition, TS also generates other products such as NO and NO_2 in the gas phase. These should also be taken into account, especially when considering the overall energy efficiency of chemical product generation by plasma interacting with water [44].

In order to improve the energy efficiency of NO_2^- production, it would be possible to achieve it by reducing the gas flow rate. If the gas flow rate is reduced from 1 l/min to 0.5 l/min. it is

necessary to use only 50% of the energy to maintain the same input energy density to produce the same amount of HNO_2 in the treated gas. In this study, however, it was not desirable to reduce the gas flow rate because the TS discharge would be less stable in humidified N_2 and would more easily switch to glow discharge. Next, it was necessary to maintain a gas flow rate of at least 1 l/min to sufficiently flush the cuvette used to measure the gaseous product concentration by UV-Vis absorption spectroscopy.

Next, we could improve the energy efficiency of NO_2^- production by improving the solvation efficiency of HNO_2 from the gas to the water microdroplets. We estimated that only about 20% of the HNO_2 molecules from the gas were captured in the PAW. If all HNO_2 molecules were used, there would be 5 times more NO_2^- ions in the water, and the energy efficiency of NO_2^- production would increase by a factor of 5. We plan to improve the HNO_2 solvation efficiency by tuning the ES process parameters (applied voltage, water flow rate). However, in this study, the water flow rate was only 500 µL/min, i.e., the same as in the experiments in the 1SR system, where TS and ES were generated simultaneously in the first section of the reactor, and the water flow rate of 500 µL/min seemed to be an optimal value taking into account the stability of the TS discharge.

4. Conclusions

Plasma activated water or plasma activated fluids are used in numerous applications. It is useful to study the interactions of plasmas generated by different discharges with water to understand the production mechanism of reactive oxygen and nitrogen species in PAW for tuning it for the desired applications. The use of microdroplets instead of bulk water to generate PAW increases the transport rate of reactive species from the gas to the water phase and has been reported in many studies.

In this study, PAW properties generated by transient spark discharge with direct and indirect treatment of electrospray microdroplets are presented. Dry or humidified synthetic air, O_2 and N_2

were used as working gas. For direct contact of the discharge with water microdroplets, TS and ES were generated simultaneously in the same section of the reactor. As a result, PAW formation was influenced by solvation of short-lived species such as OH, HO_2, or $O(^1D)$ radicals. In indirect treatment experiments, the discharge was generated in the first section and water microdroplets were generated in the second section of the reactor. Thus, the formation of PAW was only influenced by the solvation of long-lived gas species such as H_2O_2, NO_2, or HNO_2. The comparison of results from different gases and two different reactor configurations allowed us to tune the RONS compositions in PAW and helped us to understand the reaction pathways in the TS-ES system. It was found that in O_2, a significantly higher concentration of H_2O_2(aq) was observed in the reactor with direct contact of TS with ES water microdroplets, and it must be attributed to the generation of H_2O_2 in the liquid phase by short-lived species. We demonstrated that the concentration of OH(aq) is much higher in PAW generated in the reactor with direct contact of TS with ES microdroplets than in water from the experiments where TS discharge and ES microdroplets were generated in separate sections of the reactor. However, further research is needed to investigate the possible influence of other species, such as $O(^1D)$ or HO_2 radicals, on the formation of H_2O_2(aq) in PAW generated by TS in direct contact with ES microdroplets. Reactor with two sections is more suitable for production of PAW with high concentration of NO_2^-(aq). TS discharge in humidified air in the first section can produce sufficient amount of long-lived HNO_2 and NO_2 molecules to be dissolved to ES water microdroplets in the second section of the reactor. In dry air, without the formation of HNO_2, the concentration of NO_2^-(aq) in PAW was much lower than in PAW from experiments with humidified air. This supports the hypothesis that HNO_2 plays a dominant role in the production of NO_2^-(aq) in PAW generated by TS discharge in humidified air. The advantage of using two separate sections is better stability of both TS discharge and ES process. When operating together, TS discharge and ES influence each other, and both discharge and ES are less regular.

In summary, it is possible to produce PAW with high concentration of H_2O_2(aq) and no NO_2^-(aq) when TS and ES are generated simultaneously in the first section of the reactor in O_2. On the other hand, PAW with high concentration of NO_2^-(aq) with negligible amount of H_2O_2(aq) can be produced by operating TS in the first section and ES in the second section of the reactor in humidified synthetic air. Both types of PAW are suitable for different applications and the selective production of either H_2O_2(aq) or NO_2^-(aq) increases the lifetime of these reactive species in PAW.

PAW with relatively high concentration of both H_2O_2(aq) and NO_2^-(aq) can be prepared in the reactor with direct contact of TS discharge with ES water microdroplets in air. Reactions between these two species reduce their lifetime to several tens of minutes, but can lead to the formation of peroxynitrite, which is very important for the bactericidal effect of PAW. In the future, we plan further research focused on optimizing the formation of H_2O_2(aq) and NO_2^-(aq) in a buffered solution. Keeping the pH of the treated solution above 4 could increase the lifetime of H_2O_2(aq) and NO_2^-(aq) while maintaining the bactericidal effects of the prepared plasma-activated solution.

Finally, the optical emission spectra revealed another new interesting phenomenon when TS discharge is generated simultaneously with ES water microdroplets. The intensity of Fe and Fe^+ emission lines increased significantly. In order to obtain a higher concentration and lifetime of H_2O_2(aq) in PAW, it is necessary to test the use of electrodes made of another metal such as tungsten. On the other hand, the presence of Fe atoms in the water can induce Fenton reactions causing depletion of H_2O_2 favorable for biomedical applications. In addition, the improved sputtering of steel electrodes indicates that TS generated simultaneously with ES could be used for the degradation of various dyes without the addition of an external catalyst source needed to initiate Fenton reactions. Therefore, additional measurements using time-resolved optical emission spectroscopy are planned to better understand and optimize Fe and Fe^+ formation with simultaneous generation of TS and ES water microdroplets.

Acknowledgments: This work was supported by Slovak Research and Development Agency APVV-22-0247 and APVV-20-0566 and Slovak Grant Agency VEGA 1/0596/22 and 1/0822/21, and Comenius University Grant UK/206/2023.

During the preparation of this work the author(s) used “DeepL Write” service in order to improve the English level. After using this tool/service, the author(s) reviewed and edited the content as needed and take(s) full responsibility for the content of the publication.

References

[1] Z. Chen, R.-G. Xu, P. Chen, Q. Wang, Potential agricultural and biomedical applications of cold atmospheric plasma-activated liquids with self-organized patterns formed at the interface, IEEE Trans. Plasma Sci. 48 (2020) 3455–3471. https://doi.org/10.1109/TPS.2020.3019995.

[2] S. Kooshki, P. Pareek, R. Mentheour, M. Janda, Z. Machala, Efficient treatment of bio-contaminated wastewater using plasma technology for its reuse in sustainable agriculture, Environ. Technol. Innov. 32 (2023) 103287. https://doi.org/10.1016/j.eti.2023.103287.

[3] R. Jangra, K. Ahlawat, A. Dixit, R. Prakash, Efficient deactivation of aerosolized pathogens using a dielectric barrier discharge based cold-plasma detergent in environment device for good indoor air quality, Sci. Rep. 13 (2023) 10295. https://doi.org/10.1038/s41598-023-37014-2.

[4] Y. Wu, S. Yu, X. Zhang, X. Wang, J. Zhang, The Regulatory Mechanism of Cold Plasma in Relation to Cell Activity and Its Application in Biomedical and Animal Husbandry Practices, Int. J. Mol. Sci. 24 (2023) 7160. https://doi.org/10.3390/ijms24087160.

[5] M. Laroussi, Cold plasma in medicine and healthcare: The new frontier in low temperature plasma applications, Front. Phys. 8 (2020) 74. https://doi.org/10.3389/fphy.2020.00074.

[6] R. Zhou, R. Zhou, P. Wang, Y. Xian, A. Mai-Prochnow, X. Lu, P. Cullen, K.K. Ostrikov, K. Bazaka, Plasma-activated water: Generation, origin of reactive species and biological applications, J. Phys. Appl. Phys. 53 (2020) 303001. https://doi.org/10.1088/1361-6463/ab81cf.

[7] Y. Zhao, A. Patange, D. Sun, B. Tiwari, Plasma-activated water: Physicochemical properties, microbial inactivation mechanisms, factors influencing antimicrobial effectiveness, and applications in the food industry, Compr. Rev. Food Sci. Food Saf. 19 (2020) 3951–3979. https://doi.org/10.1111/1541-4337.12644.

[8] S. Pipliya, S. Kumar, N. Babar, P.P. Srivastav, Recent trends in non-thermal plasma and plasma activated water: Effect on quality attributes, mechanism of interaction and potential application in food & agriculture, Food Chem. Adv. (2023) 100249. https://doi.org/10.1016/j.focha.2023.100249.

[9] S. Herianto, R.D. Arcega, C.-Y. Hou, H.-R. Chao, C.-C. Lee, C.-M. Lin, T. Mahmudiono, H.-L. Chen, Chemical decontamination of foods using non-thermal plasma-activated water, Sci. Total Environ. 874 (2023) 162235. https://doi.org/10.1016/j.scitotenv.2023.162235.

[10] G.J. Lee, P. Lamichhane, S.J. Ahn, S.H. Kim, M.A. Yewale, C.E. Choong, M. Jang, E.H. Choi, Nitrate capture investigation in plasma-activated water and its antifungal effect on Cryptococcus pseudolongus cells, Int. J. Mol. Sci. 22 (2021) 12773. https://doi.org/10.3390/ijms222312773.

[11] N. Rao, X. Chu, K. Hadinoto, R. Zhou, T. Zhang, B. Soltani, C. Bailey, F.J. Trujillo, G. Leslie, S. Prescott, Algal cell inactivation and damage via cold plasma-activated bubbles: Mechanistic insights and process benefits, Chem. Eng. J. 454 (2023) 140304. https://doi.org/10.1016/j.cej.2022.140304s.

[12] A. Soni, J. Choi, G. Brightwell, Plasma-activated water (PAW) as a disinfection technology for bacterial inactivation with a focus on fruit and vegetables, Foods 10 (2021) 166. https://doi.org/10.3390/foods10010166.

[13] I.-E. Vlad, S.D. Anghel, Time stability of water activated by different on-liquid atmospheric pressure plasmas, J. Electrost. 87 (2017) 284–292. https://doi.org/10.1016/j.elstat.2017.06.002cold.

[14] R. Zhou, R. Zhou, K. Prasad, Z. Fang, R. Speight, K. Bazaka, K.K. Ostrikov, Cold atmospheric plasma activated water as a prospective disinfectant: The crucial role of peroxynitrite, Green Chem. 20 (2018) 5276–5284. https://doi.org/10.1039/C8GC02800A.

[15] N. Punith, R. Harsha, R. Lakshminarayana, M. Hemanth, M. S Anand, S. Dasappa, Plasma activated water generation and its application in agriculture, Adv. Mater. Lett. 10 (2019) 700–704. https://doi.org/10.5185/amlett.2019.0042.

[16] B. Šerá, V. Scholtz, J. Jirešová, J. Khun, J. Julák, M. Šerý, Effects of non-thermal plasma treatment on seed germination and early growth of leguminous plants—A review, Plants 10 (2021) 1616. https://doi.org/10.3390/plants10081616.

[17] P. Bruggeman, C. Leys, Non-thermal plasmas in and in contact with liquids, J. Phys. Appl. Phys. 42 (2009) 053001. https://doi.org/10.1088/0022-3727/42/5/053001.

[18] X. Gao, K. Huang, A. Zhang, C. Wang, Z. Sun, Y. Liu, Simultaneous degradation of glucocorticoids and sterilization using bubbling corona discharge plasma based systems: a promising terminal water treatment facility for hospital wastewater, Chem. Eng. J. 430 (2022) 132845. https://doi.org/10.1016/j.cej.2021.132845.

[19] B. Jiang, J. Zheng, S. Qiu, M. Wu, Q. Zhang, Z. Yan, Q. Xue, Review on electrical discharge plasma technology for wastewater remediation, Chem. Eng. J. 236 (2014) 348–368. https://doi.org/10.1016/j.cej.2013.09.090.

[20] P. Lamichhane, T.R. Acharya, N. Kaushik, L.N. Nguyen, J.S. Lim, V. Hessel, N.K. Kaushik, E.H. Choi, Non-thermal argon plasma jets of various lengths for selective reactive oxygen and nitrogen species production, J. Environ. Chem. Eng. 10 (2022) 107782. https://doi.org/10.1016/j.jece.2022.107782.

[21] M.J. Pavlovich, D.S. Clark, D.B. Graves, Quantification of air plasma chemistry for surface disinfection, Plasma Sources Sci. Technol. 23 (2014) 065036. https://doi.org/10.1088/0963-0252/23/6/065036.

[22] L. Nani, F. Tampieri, E. Ceriani, E. Marotta, C. Paradisi, ROS production and removal of the herbicide metolachlor by air non-thermal plasma produced by DBD, DC− and DC+ discharges implemented within the same reactor, J. Phys. Appl. Phys. 51 (2018) 274002. https://doi.org/10.1088/1361-6463/aab8b9.

[23] Z. Machala, B. Tarabová, D. Sersenová, M. Janda, K. Hensel, Chemical and antibacterial effects of plasma activated water: Correlation with gaseous and aqueous reactive oxygen and nitrogen species, plasma sources and air flow conditions, J. Phys. Appl. Phys. 52 (2018) 034002. https://doi.org/10.1088/1361-6463/aae807.

[24] Y. Yang, Z. Li, L. Nie, X. Lu, Effect of liquid-dissolved gas components on concentrations of the aqueous reactive oxygen and nitrogen species, J. Appl. Phys. 125 (2019). https://doi.org/10.1063/1.5085258.

[25] P. Bruggeman, M.J. Kushner, B.R. Locke, J.G. Gardeniers, W. Graham, D.B. Graves, R. Hofman-Caris, D. Maric, J.P. Reid, E. Ceriani, Plasma–liquid interactions: a review and roadmap, Plasma Sources Sci. Technol. 25 (2016) 053002. https://doi.org/10.1088/0963-0252/25/5/053002.

[26] J. Kruszelnicki, A.M. Lietz, M.J. Kushner, Atmospheric pressure plasma activation of water droplets, J. Phys. Appl. Phys. 52 (2019) 355207. https://doi.org/10.1088/1361-6463/ab25dc.

[27] M.E. Hassan, M. Janda, Z. Machala, Transport of gaseous hydrogen peroxide and ozone into bulk water vs. electrosprayed aerosol, Water 13 (2021) 182. https://doi.org/10.3390/w13020182.

[28] R. Pietro, G. McGovern, H.T.K. Tse, A. Fulmer, M. Kovalenko, G. Nirenberg, V. Miller, A. Rabinovich, A. Fridman, G. Fridman, Microsecond-Pulsed Dielectric Barrier Discharge Plasma-Treated Mist for Inactivation of Escherichia coli In Vitro, IEEE Trans. Plasma Sci. 47 (2019) 395–402. https://doi.org/10.1109/TPS.2018.2878971.

[29] N.S. Chew, C.W. Ooi, L.Y. Yeo, M.K. Tan, Hybrid atmospheric pressure plasma generation and DC electrospray aerosolization of plasma-activated water for surface pathogen disinfection, Plasma Process. Polym. 20 (2023) 2200128. https://doi.org/10.1002/ppap.202200128.

[30] N.S. Chew, K.S. Wong, W.S. Chang, C.W. Ooi, L.Y. Yeo, M.K. Tan, Nanoscale plasma-activated aerosol generation for in situ surface pathogen disinfection, Microsyst. Nanoeng. 8 (2022) 41. https://doi.org/10.1038/s41378-022-00373-3.

[31] J. Zeleny, The electrical discharge from liquid points, and a hydrostatic method of measuring the electric intensity at their surfaces, Phys. Rev. 3 (1914) 69. https://doi.org/10.1103/PhysRev.3.69.

[32] J. Zeleny, Instability of electrified liquid surfaces, Phys. Rev. 10 (1917) 1. https://doi.org/10.1103/PhysRev.10.1.

[33] A. Jaworek, Electrospray droplet sources for thin film deposition, J. Mater. Sci. 42 (2007) 266–297. https://doi.org/10.1007/s10853-006-0842-9.

[34] C. Carotenuto, F. Di Natale, A. Lancia, Wet electrostatic scrubbers for the abatement of submicronic particulate, Chem. Eng. J. 165 (2010) 35–45. https://doi.org/10.1016/j.cej.2010.08.049.

[35] A.K. Ball, S.S. Roy, D.R. Kisku, N.C. Murmu, L. dos Santos Coelho, Optimization of drop ejection frequency in EHD inkjet printing system using an improved Firefly Algorithm, Appl. Soft Comput. 94 (2020) 106438. https://doi.org/10.1016/j.asoc.2020.106438.

[36] J.-P. Borra, P. Ehouarn, D. Boulaud, Electrohydrodynamic atomisation of water stabilised by glow discharge—operating range and droplet properties, J. Aerosol Sci. 35 (2004) 1313–1332. https://doi.org/10.1016/j.jaerosci.2004.05.011.

[37] W. Bian, M. Zhou, L. Lei, Formations of active species and by-products in water by pulsed high-voltage discharge, Plasma Chem. Plasma Process. 27 (2007) 337–348. https://doi.org/10.1007/s11090-007-9066-2.

[38] Z. Kovalova, M. Leroy, M.J. Kirkpatrick, E. Odic, Z. Machala, Corona discharges with water electrospray for Escherichia coli biofilm eradication on a surface, Bioelectrochemistry 112 (2016) 91–99. https://doi.org/10.1016/j.bioelechem.2016.05.002.

[39] B. Tarabová, P. Lukeš, E. Doležalová, R. Menthéour, Z. Machala, Bactericidal effects induced by air transient spark with electrospray and/or PAW linked with RONS chemistry enhanced by other plasma agents, (n.d.).

[40] M. Janda, K. Hensel, P. Tóth, M.E. Hassan, Z. Machala, The role of HNO2 in the generation of plasma-activated water by air transient spark discharge, Appl. Sci. 11 (2021) 7053. https://doi.org/10.3390/app11157053.

[41] M. Janda, V. Martišovitš, Z. Machala, Transient spark: a dc-driven repetitively pulsed discharge and its control by electric circuit parameters, Plasma Sources Sci. Technol. 20 (2011) 035015. https://doi.org/10.1088/0963-0252/20/3/035015.

[42] M. Janda, Z. Machala, A. Niklová, V. Martišovitš, The streamer-to-spark transition in a transient spark: a dc-driven nanosecond-pulsed discharge in atmospheric air, Plasma Sources Sci. Technol. 21 (2012) 045006. https://doi.org/10.1088/0963-0252/21/4/045006.

[43] M. Janda, V. Martišovitš, K. Hensel, L. Dvonč, Z. Machala, Measurement of the electron density in transient spark discharge, Plasma Sources Sci. Technol. 23 (2014) 065016. https://doi.org/10.1088/0963-0252/23/6/065016.

[44] J. Luo, L. Nie, D. Liu, X. Lu, Electrodeless discharge in water: Reactive species in liquid and gas phase and energy cost for nitrogen fixation, Plasma Process. Polym. 20 (2023) 2200181. https://doi.org/10.1002/ppap.202200181.

[45] M. Janda, K. Hensel, Z. Machala, T.A. Field, The influence of electric circuit parameters on NOx generation by transient spark discharge, J. Phys. Appl. Phys. 56 (2023) 485202. https://doi.org/10.1088/1361-6463/ace634.

[46] A. Kramida, Yu. Ralchenko, J. Reader, NIST ASD Team, NIST Atomic Spectra Database (version 5.8), (2020). https://doi.org/10.18434/T4W30F.

[47] C.O. Laux, Radiation and nonequilibrium collisional-radiative models Physico-Chemical Modeling of High Enthalpy and Plasma Flows (Lecture Series 2002–07), Rhode-Saint-Gense, Belgium: von Karman Institute, 2002.

[48] H. Keller-Rudek, G. Moortgat, R. Sander, R. Sörensen, The MPI-Mainz UV/VIS spectral atlas of gaseous molecules of atmospheric interest, Earth Syst. Sci. Data 5 (2013) 365–373. https://doi.org/10.5194/essd-5-365-2013.

[49] P. Lukes, E. Dolezalova, I. Sisrova, M. Clupek, Aqueous-phase chemistry and bactericidal effects from an air discharge plasma in contact with water: evidence for the formation of peroxynitrite through a pseudo-second-order post-discharge reaction of H2O2 and HNO2, Plasma Sources Sci. Technol. 23 (2014) 015019.

[50] H. Jablonowski, M.A.C. Hänsch, M. Dünnbier, K. Wende, M.U. Hammer, K.-D. Weltmann, S. Reuter, T. von Woedtke, Plasma jet's shielding gas impact on bacterial inactivation, Biointerphases 10 (2015) 029506. https://doi.org/10.1116/1.4916533.

[51] G. Mark, A. Tauber, R. Laupert, H.-P. Schuchmann, D. Schulz, A. Mues, C. von Sonntag, OH-radical formation by ultrasound in aqueous solution–Part II: Terephthalate and Fricke dosimetry and the influence of various conditions on the sonolytic yield, Ultrason. Sonochem. 5 (1998) 41–52. https://doi.org/10.1016/S1350-4177(98)00012-1.

[52] P. Attri, Y.H. Kim, D.H. Park, J.H. Park, Y.J. Hong, H.S. Uhm, K.-N. Kim, A. Fridman, E.H. Choi, Generation mechanism of hydroxyl radical species and its lifetime prediction during the plasma-initiated ultraviolet (UV) photolysis, Sci. Rep. 5 (2015) 1–8. https://doi.org/10.1038/srep09332.

[53] S. Kanazawa, T. Furuki, T. Nakaji, S. Akamine, R. Ichiki, Application of chemical dosimetry to hydroxyl radical measurement during underwater discharge, in: IOP Publishing, 2013: p. 012102. https://doi.org/10.1088/1742-6596/418/1/012102.

[54] V. Veronico, P. Favia, F. Fracassi, R. Gristina, E. Sardella, Validation of colorimetric assays for hydrogen peroxide, nitrate and nitrite ions in complex plasma-treated water solutions, Plasma Process. Polym. 18 (2021) 2100062. https://doi.org/10.1002/ppap.202100062.

[55] Z. Machala, I. Jedlovsky, V. Martisovits, DC discharges in atmospheric air and their transitions, IEEE Trans. Plasma Sci. 36 (2008) 918–919. https://doi.org/10.1109/TPS.2008.922488.

[56] A. Komuro, R. Ono, T. Oda, Behaviour of OH radicals in an atmospheric-pressure streamer discharge studied by two-dimensional numerical simulation, J. Phys. Appl. Phys. 46 (2013) 175206. https://doi.org/10.1088/0022-3727/46/17/175206toxi.

[57] C.C. Winterbourn, Toxicity of iron and hydrogen peroxide: the Fenton reaction, Toxicol. Lett. 82 (1995) 969–974. https://doi.org/10.1016/0378-4274(95)03532-X.

[58] S. Jodzis, K. Baran, The influence of gas temperature on ozone generation and decomposition in ozone generator. How is ozone decomposed?, Vacuum 195 (2022) 110647. https://doi.org/10.1016/j.vacuum.2021.110647.

[59] D.-X. Liu, P. Bruggeman, F. Iza, M.-Z. Rong, M.G. Kong, Global model of low-temperature atmospheric-pressure He+ H2O plasmas, Plasma Sources Sci. Technol. 19 (2010) 025018. https://doi.org/10.1088/0963-0252/19/2/025018.

[60] K. Takahashi, Y. Takeuchi, Y. Matsumi, Rate constants of the O (1D) reactions with N2, O2, N2O, and H2O at 295 K, Chem. Phys. Lett. 410 (2005) 196–200. https://doi.org/10.1016/j.cplett.2005.05.062.

[61] A.S. Viner, P.A. Lawless, D.S. Ensor, L.E. Sparks, Ozone generation in DC-energized electrostatic precipitators, IEEE Trans. Ind. Appl. 28 (1992) 504–512. https://doi.org/10.1109/28.137427.

[62] K.C. Hsieh, R.J. Wandell, S. Bresch, B.R. Locke, Analysis of hydroxyl radical formation in a gas-liquid electrical discharge plasma reactor utilizing liquid and gaseous radical scavengers, Plasma Process. Polym. 14 (2017) 1600171. https://doi.org/10.1002/ppap.201600171.

[63] M. Capitelli, C.M. Ferreira, B.F. Gordiets, A.I. Osipov, Plasma Kinetics in Atmospheric Gases, Springer, 2000.

[64] Y. Gorbanev, D. O'Connell, V. Chechik, Non-thermal plasma in contact with water: The origin of species, Chem. Eur. J. 22 (2016) 3496–3505. https://doi.org/10.1002/chem.201503771.

[65] S. Kanazawa, H. Kawano, S. Watanabe, T. Furuki, S. Akamine, R. Ichiki, T. Ohkubo, M. Kocik, J. Mizeraczyk, Observation of OH radicals produced by pulsed discharges on the surface of a liquid, Plasma Sources Sci. Technol. 20 (2011) 034010. https://doi.org/10.1088/0963-0252/20/3/034010.

[66] P. Bruggeman, D.C. Schram, On OH production in water containing atmospheric pressure plasmas, Plasma Sources Sci. Technol. 19 (2010). https://doi.org/10.1088/0963-0252/19/4/045025.

[67] X. Zhou, Z. Zhao, J. Liang, H. Yuan, W. Wang, D. Yang, Measurement of reactive species in different solutions of bubble discharge with varying O2/N 2 proportion in Ar: Analysis of

reaction pathways, Plasma Process. Polym. 16 (2019) e1900001. https://doi.org/10.1002/ppap.201900001.

[68] B.R. Locke, K.-Y. Shih, Review of the methods to form hydrogen peroxide in electrical discharge plasma with liquid water, Plasma Sources Sci. Technol. 20 (2011) 034006. https://doi.org/10.1088/0963-0252/20/3/034006.

[69] H. Taube, Photochemical reactions of ozone in solution, Trans. Faraday Soc. 53 (1957) 656–665. https://doi.org/10.1039/TF9575300656.

[70] S. Xu, V. Jirasek, P. Lukes, Molecular dynamics simulations of singlet oxygen atoms reactions with water leading to hydrogen peroxide, J. Phys. Appl. Phys. 53 (2020) 275204. https://doi.org/10.1088/1361-6463/ab8321.

[71] K. Shimada, K. Takashima, Y. Kimura, K. Nihei, H. Konishi, T. Kaneko, Humidification effect of air plasma effluent gas on suppressing conidium germination of a plant pathogenic fungus in the liquid phase, Plasma Process. Polym. 17 (2020) 1900004. https://doi.org/10.1002/ppap.201900004.

[72] S. Ikawa, A. Tani, Y. Nakashima, K. Kitano, Physicochemical properties of bactericidal plasma-treated water, J. Phys. Appl. Phys. 49 (2016) 425401. https://doi.org/10.1088/0022-3727/49/42/425401.

[73] H. Cheng, J. Luo, K. Song, F. Zhao, D. Liu, L. Nie, X. Lu, On the dose of plasma medicine: Plasma-activated medium (PAM) and its effect on cell viability, Phys. Plasmas 29 (2022). https://doi.org/10.1063/5.0089357.

[74] E. Tsoukou, P. Bourke, D. Boehm, Temperature stability and effectiveness of plasma-activated liquids over an 18 months period, Water 12 (2020) 3021. https://doi.org/10.3390/w12113021.

[75] K. Tachibana, T. Nakamura, Comparative study of discharge schemes for production rates and ratios of reactive oxygen and nitrogen species in plasma activated water, J. Phys. Appl. Phys. 52 (2019) 385202. https://doi.org/10.1088/1361-6463/ab2529.

[76] N. Bolouki, W.-H. Kuan, Y.-Y. Huang, J.-H. Hsieh, Characterizations of a plasma-water system generated by repetitive microsecond pulsed discharge with air, nitrogen, oxygen, and argon gases species, Appl. Sci. 11 (2021) 6158. https://doi.org/10.3390/app11136158.

[77] Z. Xu, X. Zhou, W. Yang, Y. Zhang, Z. Ye, S. Hu, C. Ye, Y. Li, Y. Lan, J. Shen, In vitro antimicrobial effects and mechanism of air plasma-activated water on Staphylococcus aureus biofilm, Plasma Process. Polym. 17 (2020) 1900270. https://doi.org/10.1002/ppap.201900270.

[78] H. Wang, R. Han, M. Yuan, Y. Li, Z. Yu, P.J. Cullen, D. Qijing, Y. Yang, J. Wang, Evaluation of plasma-activated water: Efficacy, stability, physicochemical properties, and mechanism of inactivation against Escherichia coli, LWT 184 (2023) 114969. https://doi.org/10.1016/j.lwt.2023.114969.

[79] C. Sarangapani, L. Scally, M. Gulan, P. Cullen, Dissipation of pesticide residues on grapes and strawberries using plasma-activated water, Food Bioprocess Technol. 13 (2020) 1728–1741. https://doi.org/10.1007/s11947-020-02515-9.